

Modelling the Key Material Properties of Germanium for Device Simulation in Cryogenic Environments

Luke J. Bradley, Alton B. Horsfall, and Angela Dyson

Abstract - Germanium is commonly suggested as an alternative for power electronic devices in emerging liquid hydrogen applications. Despite the clear benefits of a two fold conductivity increase and fabrication familiarity within the community, very few models exist that describe the temperature dependent electrical characteristics of the material. Here, models are presented and adapted which describe the temperature and doping dependence of the carrier concentration, mobility, and velocity from room temperature down to 20 K. For each of these, closed-loop models are adapted that can be readily used in technology computer aided design (TCAD) software and new models are introduced when required. For high-field applications, the carrier velocity has been independently considered for both the $\langle 100 \rangle$ and $\langle 111 \rangle$ directions with the introduction of a new model for electrons in the $\langle 100 \rangle$ direction. With the work conducted here, it is now possible to simulate and predict the performance and suitability of germanium electronics for emerging low and high power applications.

Index Terms—Germanium, Semiconductor device modeling, Charge carrier mobility, Charge carrier density, Cryogenic electronics.

I. INTRODUCTION

In an effort to further reduce greenhouse emissions, companies and researchers are looking into the integration of liquid hydrogen fuel cells into aerospace and automotive vehicles [1], [2]. These applications incorporate high temperature superconductors to form DC busses with supply voltage ranging from 15 V to 1.3 kV [1], [3]. Normally, power electronic devices fabricated from silicon, 4H-SiC and GaN would be the devices/materials of choice for use in control circuits supporting these voltages, but this is not the case for emerging liquid hydrogen where these devices become extremely resistive due to the cryogenic environment [4], [5]. In contrast, the experimental data for devices fabricated from germanium are shown to still operate at 4 K with room temperature like characteristics [6], [7].

For germanium, a vast concentration of experimental papers have been published analysing the carrier concentration, mobility and thermal conductivity that highlight the

The work of L.J. Bradley (Corresponding author: Luke.Bradley@newcastle.ac.uk) was supported by the Engineering and Physical Sciences Research Council (EPSRC) through a Scholarship under Award Ref 1665165.

The authors L.J. Bradley and A. Dyson (Angela.Dyson@newcastle.ac.uk) are with the School of Engineering and School of Maths, Statics and Physics respectively at Newcastle University, UK whilst A.B. Horsfall (alton.b.Horsfall@durham.ac.uk) is with the Department of Engineering at Durham University, UK.

attractive conductive and thermal properties of the material [8]–[12]. As examples, the electron mobility and thermal conductivity rise from 3900 cm²/Vs and 0.48 W/cmK at room temperature to over 10⁶ cm²/Vs and 10 W/cmK at 20 K respectively. Due to the superior room temperature properties of silicon however, coupled with the superior stability of native SiO₂ in comparison to water soluble GeO₂, models used to describe the temperature, doping and field dependence of the carrier concentration and mobility are scarce in comparison to the widely accepted and commonly used silicon models. As such, manufacturers and experimentalists must iteratively manufacture germanium devices to predict optimal device structures to minimise device size and resistance.

In recent years however, advancements in germanium contacting [13] and alternative high- κ dielectrics [14], [15] have resulted in a large increase in publications of high quality lateral MOSFETs with stable oxides that have greater carrier mobilities than their silicon counterparts. As well as MOSFETs, germanium shows promise for low resistance medium power applications in the operating range of 25 to 500 V when incorporating liquid hydrogen fuel cells due to the superior material conductivity at these temperatures.

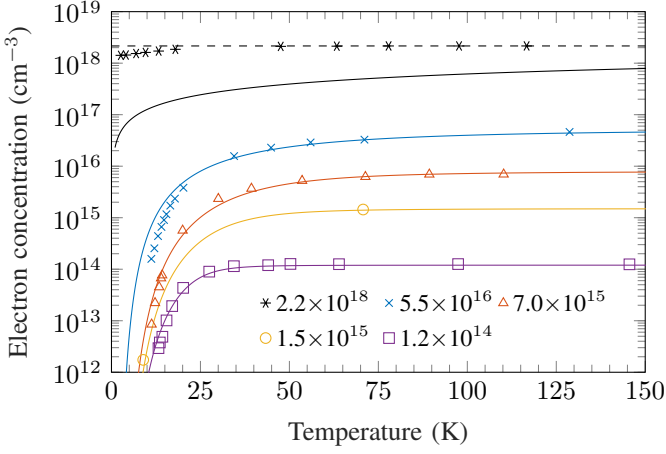
Here, the carrier concentration, mobility and velocity within near intrinsic to degenerately doped germanium has been modelled as a function of temperature and doping from 20 K to room temperature. The direction dependence of the carrier velocity for high power devices has also been considered which now makes it possible to simulate the performance of power devices based on germanium for emerging high power applications.

II. CARRIER CONCENTRATION

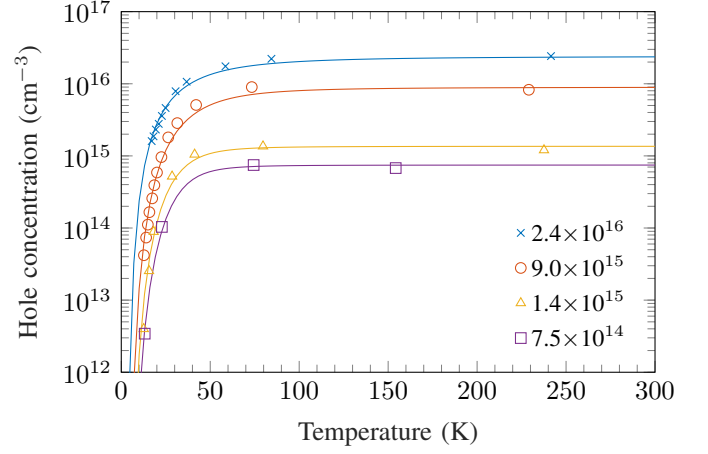
It has previously been shown [16] that at cryogenic temperatures, the free carrier concentration for a non-degenerate semiconductor can be modelled through

$$n_{\text{app}} = \frac{N_C \left(\sqrt{1 + 4 \frac{N_D}{N_C} g_D \exp\left(\frac{\Delta E_{D,\text{app}}}{k_B T}\right)} - 1 \right)}{2g_D \exp\left(\frac{\Delta E_{D,\text{app}}}{k_B T}\right)} \quad (1)$$

where N_C is the density of states in the conduction band, N_D is the donor concentration, g_D is the electron degeneracy factor, $k_B T$ is the thermal energy and $\Delta E_{D,\text{app}}$ is the difference between the conduction band minimum and donor energy level. The subscript 'app' is used to emphasise that



(a) Calculated electron concentration for different net donor concentrations compared to experimental data (x, Δ , \square [8], \circ [9], * [10])



(b) Calculated hole concentration for different net acceptor concentrations compared to experimental data [11]

Fig. 1: Electron and hole concentrations in germanium assuming a negligible compensation ratio. Dashed line for electron concentration highlights assumption that $n = N_D$.

the concentration is based on the *apparent* ionisation energy through the assumption that there is a negligible acceptor concentration. When deriving Eq. (1), the parallel equation for holes can be derived by replacing all of the n-type terms with the p-type equivalent terms.

A plot of the apparent electron and hole concentrations within antimony and gallium doped germanium is plotted in Fig. 1 based on the published net doping concentrations. Like previous work on silicon and 4H-SiC [19], [20], it was found that the donor and acceptor ionisation energies had to be corrected for the reduction in ionisation energy at higher doping concentrations. Based on fitting to the experimental data for germanium, it was found that previous models overestimate the reduction in ionisation energy for both donors and acceptors in germanium [19], [20]. For antimony and gallium in germanium, the resulting free

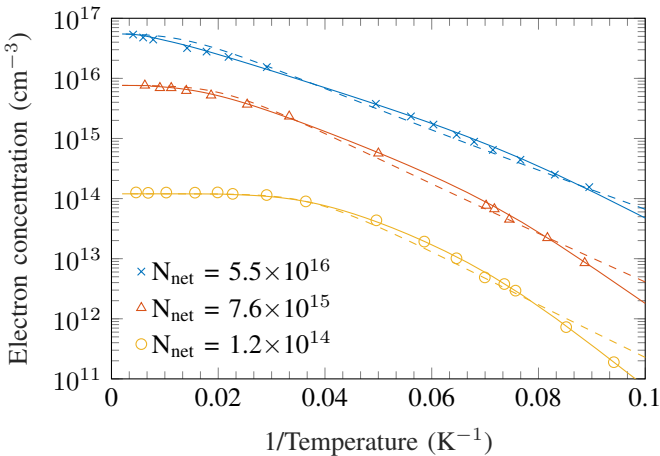
carrier concentrations can be modelled using

$$E_{D,app} = E_{D,0} - 1.22 \times 10^{-19} N_{net} + 2.99 \times 10^{-37} N_{net}^2 \quad (2)$$

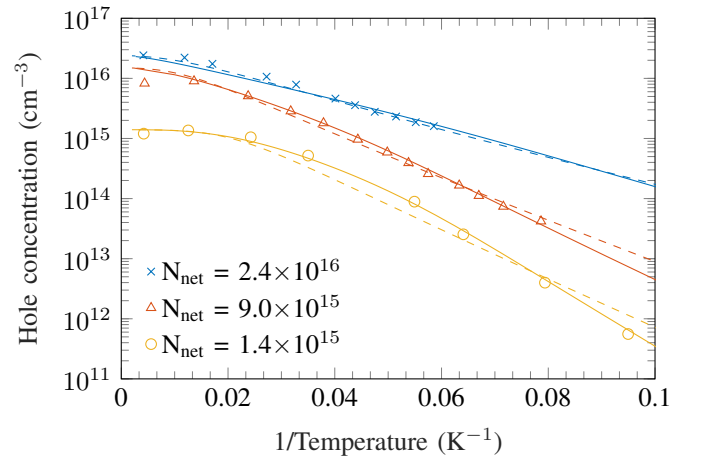
and

$$E_{A,app} = E_{A,0} - 5.65 \times 10^{-19} N_{net} + 9.12 \times 10^{-36} N_{net}^2 \quad (3)$$

where N_{net} is the difference in the majority and the minority dopant concentration. For doping concentrations exceeding 10^{17} cm^{-3} , the ionisation energy reduces to zero as the donor/acceptor impurity band overlaps with the conduction/valence band edge and so the carriers no longer require excitation to become available for conduction. For such a case, the semiconductor can be assumed to be fully ionised as can be seen for the experimental data for an antimony concentration of $2.2 \times 10^{18} \text{ cm}^{-3}$.



(a) Electron concentration [8] where N_{net} is equal to $N_D - N_A$



(b) Hole concentration [11] where N_{net} is equal to $N_A - N_D$

Fig. 2: Comparison of uncompensated model (dashed) to compensated model (solid) used to calculate carrier concentration in comparison to experimental data for electron (a) and hole concentrations (b).

Table I: Concentrations and energies used to fit data for electron and hole concentrations in Fig. 1 and 2. For the closed loop approximation the minority doping concentration is assumed to be zero and the ionisation energy is given by $E_{D,app}$ or $E_{A,app}$. For the numeric model, the ionisation energy is given by $E_{D,num}$ or $E_{A,num}$.

$N_D - N_A$ (cm^{-3})	N_A (cm^{-3})	$E_{D,app}$ (eV)	$E_{D,num}$ (eV)	$N_A - N_D$ (cm^{-3})	N_D (cm^{-3})	$E_{A,app}$ (eV)	$E_{A,num}$ (eV)
1.2×10^{14}	1.0×10^{13}	0.016	0.013	1.4×10^{15}	2.8×10^{14}	0.015	0.009
7.6×10^{15}	1.5×10^{14}	0.015	0.011	1.5×10^{16}	3.0×10^{15}	0.012	0.007
5.5×10^{16}	1.3×10^{15}	0.012	0.008	2.4×10^{16}	4.8×10^{15}	0.008	0.004

For a select few data sets within Fig. 1, a discrepancy can be seen between the apparent carrier concentration model and the experimental data within the freeze-out region. At low temperatures, the exponential term within Eq. (1) dominates and the apparent carrier concentration can be reduced to

$$n = \sqrt{\frac{N_D N_C}{g_D}} \exp\left(-\frac{\Delta E_{D,app}}{2k_B T}\right) \quad (4)$$

It has been pointed out previously [21] that for a non-negligible minority concentration, within the freeze-out region, the carrier concentration must be calculated numerically using

$$\frac{n_{num}(N_A + n_{num})}{N_D - N_A - n_{num}} = \frac{N_C}{g_D} \exp\left(-\frac{\Delta E_{D,num}}{k_B T}\right) \quad (5)$$

A comparison of the apparent and numerical models is plotted in Fig. 2. For electrons and holes, the conduction and valence band density of states effective mass were equal to $0.3m_0$ and $0.2m_0$ respectively for both models. From fitting the numeric model to the data, it was also found that the ionisation energies were lower than all values used in the best fit of the closed loop approximation. A list of the minority donor/acceptor concentration and energies for the two models are given in Table I. From the Arrhenius plot, it can be seen that the closed loop approximation of the carrier concentration results in a straight line where the slope is proportional to the ionisation energy. In comparison to the experimental data, it can be seen that although the

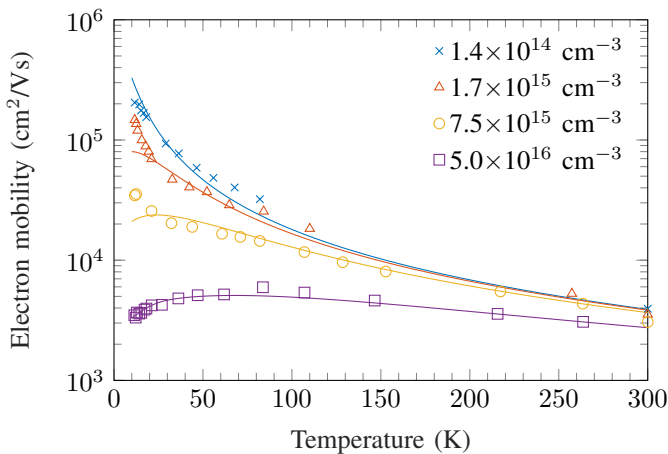
measured data remains within close proximity of the closed loop approximation, the presence of compensating impurities leads to a non-linear gradient that is predicted well by the numerical model.

For temperatures below 20 K, i.e. for liquid hydrogen or space applications, the numerical method for calculating the carrier concentrations must be employed. For emerging liquid hydrogen applications, the error between the closed loop approximation model and the numeric model is less than 25% at 20 K and so the closed loop model becomes suitable for regions of low to moderate doping concentrations.

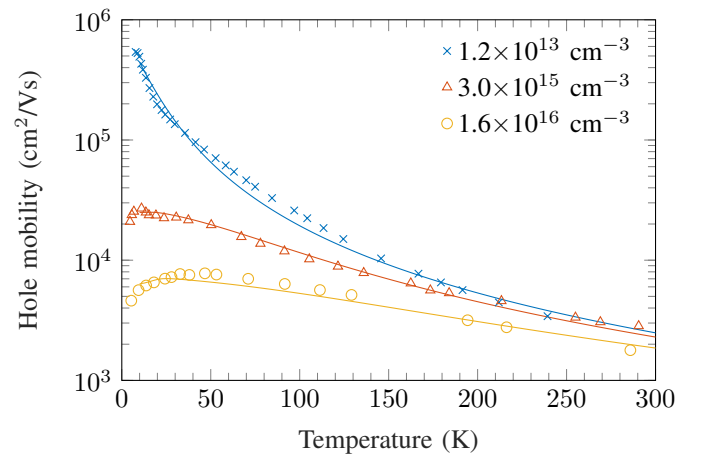
III. CARRIER MOBILITY

As with silicon and 4H-SiC, the carrier mobility in germanium varies greatly with field, temperature and doping concentration. Previous works have shown that the carrier mobility can be accurately modelled through the numerical averaging of the scattering rates from phonons and impurities, although this method is impractical for device simulation proposes where these properties and the effective electric field can vary with location within a device. For example, in high field germanium MOS devices, the increased scattering from the transverse field F_{\perp} from high gate biases is well documented [15].

Within TCAD, there exists a low field mobility model which includes the aforementioned scattering mechanisms for majority and minority carriers in semiconductors as a function of temperature and both ionised acceptor and donor concentrations [26]. The low field mobility model, known as



(a) n-type TCAD mobility model compared to experimental data [8]



(b) p-type TCAD mobility model compared to experimental data [17], [18]

Fig. 3: Mobility model used in TCAD simulations for Ge as a function of temperature and doping compared to experimental data at low fields.

the *Philips unified mobility model*, is given by

$$\frac{1}{\mu_i} = \frac{1}{\mu_{i,L}} + \frac{1}{\mu_{i,A}} \quad (6)$$

where $\mu_{i,L}$ represents the doping independent lattice scattering mobility equal to

$$\mu_{i,L} = \mu_{i,\max} \left(\frac{T}{300} \right)^{-\theta_i} \quad (7)$$

where $\mu_{i,\max}$ and θ are fitting constants and the subscript 'i' is altered to 'e' for electrons or 'h' for holes. $\mu_{i,A}$ is the mobility calculated from a model which takes into account all other scattering mechanisms through

$$\mu_{i,A} = \mu_{i,N} \left(\frac{N_{i,sc}}{N_{i,sc,eff}} \right) \left(\frac{N_{i,ref}}{N_{i,sc}} \right)^{\alpha_i} + \mu_{i,c} \left(\frac{n+p}{N_{i,sc,eff}} \right) \quad (8)$$

where $N_{i,ref}$, $N_{i,sc}$ and $N_{i,sc,eff}$ are all fitting terms based on carrier densities and

$$\mu_{i,N} = \frac{\mu_{i,\max}^2}{\mu_{i,\max} - \mu_{i,\min}} \left(\frac{T}{300} \right)^{3\alpha_i - 1.5} \quad (9a)$$

$$\mu_{i,c} = \frac{\mu_{i,\max} \mu_{i,\min}}{\mu_{i,\max} - \mu_{i,\min}} \left(\frac{300}{T} \right)^{0.5} \quad (9b)$$

are used as fitting terms when comparing the model to experimental data.

The model was originally developed for calculating the carrier mobility in silicon devices at a given temperature assuming that the donor, acceptor, electron and hole concentrations were all known [26] and can therefore be adapted to model the carrier mobility of germanium using experimental data as shown in Fig. 3.

For modelling the carrier mobility in germanium, the values for μ_{\min} and μ_{\max} were taken from the maximum and minimum carrier mobilities at room temperature as a function of doping concentration. Considering experimental mobilities, the maximum and minimum values obtained are 3900 and 120 cm²/Vs for electrons [27] and 2250 and

100 cm²/Vs for holes [28]. To determine the temperature dependence of lattice scattering limited mobility, the exponent θ must be taken from the average of the optical and acoustic scattering limited carrier mobility at low doping concentrations by considering the low doped electron and hole mobility data in figure 3.

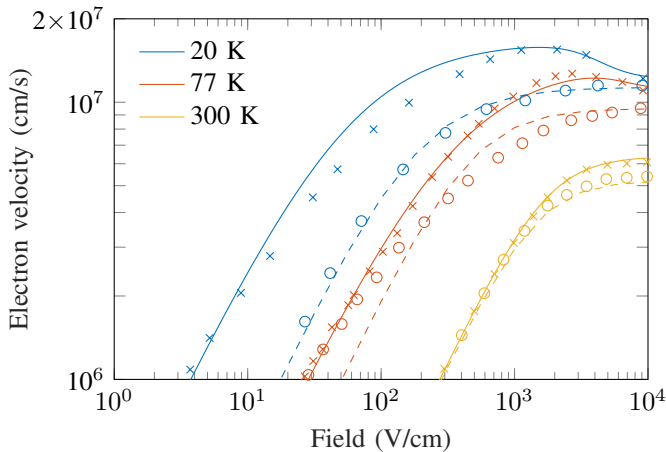
Using a non linear least square fitting method, the value for θ was calculated as 1.65 and 2 for electrons and holes respectively which is in good agreement for electrons based on previous work [29], [30] and the values for α and $N_{i,ref}$ were found to be 0.55 for both electrons and holes and 3×10^{17} and 4×10^{17} cm⁻³ for electrons and holes respectively.

A plot of the mobility model as a function of both temperature and doping concentration is plotted in Fig. 3. From the figure, it can be seen that the model has been successfully adapted to take into account the temperature and doping dependence of the electron and hole mobilities in germanium. Consistent with what is found in literature, the temperature dependence of the carrier mobility reduces with increasing doping concentration whilst samples with low doping concentrations are dominated by the lattice scattering mobility given by Eq. (7). At temperatures below 20 K, the electron mobility for samples doped at 1.7×10^{15} and 7.5×10^{15} cm⁻³ continues to increase in contrast to what is predicted by the model. As the focus of this work was on the modelling of devices at 20 K and above, this inconsistency was not explored further.

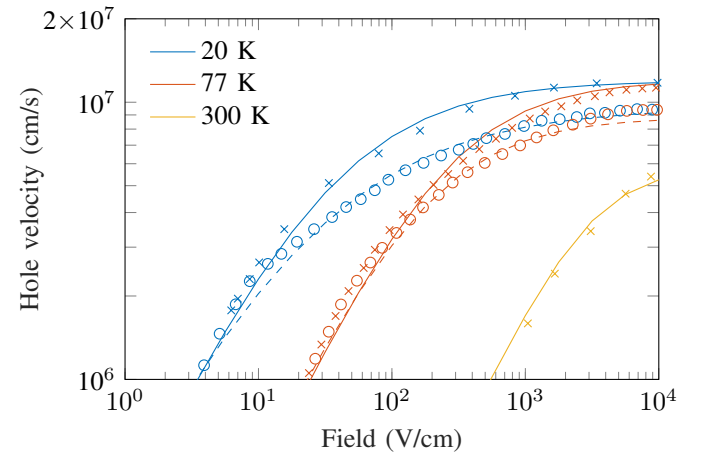
Regardless, the adapted model is suitable for modelling the carrier mobility within germanium for electrons and holes at temperatures between 20 and 300 K.

IV. VELOCITY SATURATION

Like silicon and 4H-SiC, at high fields, the carrier velocity in germanium reduces at high fields before saturating to a constant value. Unlike silicon and 4H-SiC however, experimental measurements show that the carrier velocity in the $\langle 100 \rangle$ direction begins to decrease at high fields



(a) Experimental and modelled electron velocity in n-type germanium [22]



(b) Experimental and modelled hole velocity in p-type germanium [23]–[25]

Fig. 4: Experimental data for the electron velocity in n-type (a) and the hole velocity in p-type germanium (b) in comparison to the presented models. Crosses and open circles indicate experimental data for the $\langle 100 \rangle$ and $\langle 111 \rangle$ directions respectively.

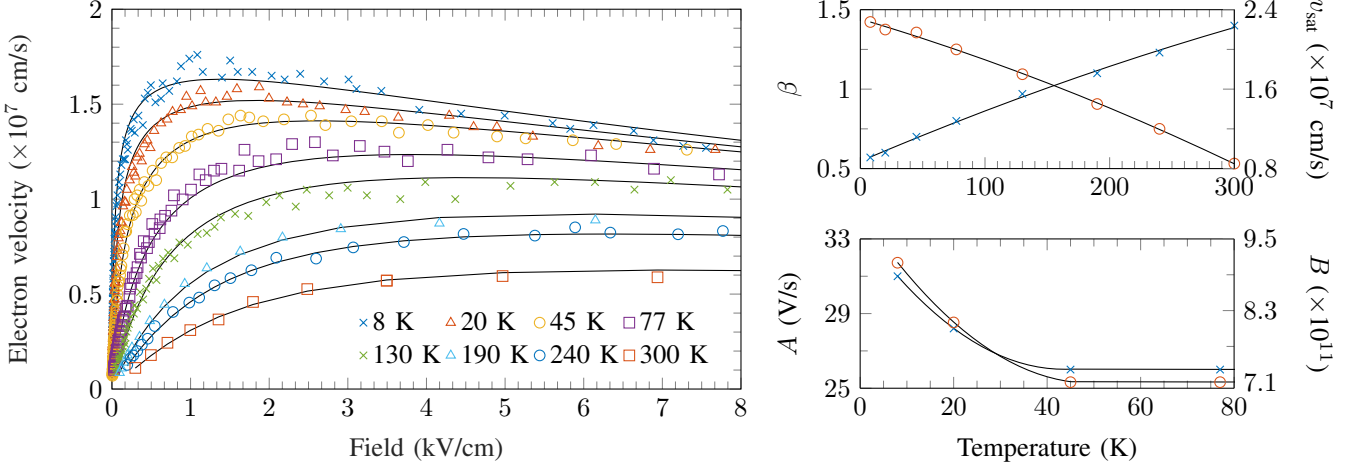


Fig. 5: Electron velocity in $\langle 100 \rangle$ from 8 K to room temperature and compared to the new high field model (Eq. (13)). Also shown is the temperature dependence of the fitting parameters β , v_{sat} , A and B . A and B are only shown from 0 to 80 K as they remain temperature independent from 45 K to room temperature.

at temperatures below 130 K due to the transfer electron effect [22]. As such, this effect must be considered at low temperatures to accurately predict device performance.

The field dependence of the carrier mobility can be modelled empirically using the models that are pre-built into TCAD. For the majority of mobility cases, the carrier velocity can be described using the extended Canali model [31]

$$\mu(F) = \frac{(\alpha + 1)\mu_{\text{low}}}{\alpha + \left[1 + \left(\frac{(\alpha+1)\mu_{\text{low}}F}{v_{\text{sat}}}\right)^\beta\right]^{1/\beta}} \quad (10)$$

where F is the applied electric field, μ_{low} is the low field mobility given by Eq. (6) and β is a temperature dependant fitting parameter given as

$$\beta = \beta_0 \left(\frac{T}{300K}\right)^{\beta_{\text{exp}}} \quad (11)$$

where β_0 and β_{exp} are fitting constants. The saturation velocity for electrons and holes in all cases were found to decrease linearly with temperature according to

$$v_{\text{sat}}(T) = A_{v,\text{sat}} - B_{v,\text{sat}} \left(\frac{T}{300K}\right) \quad (12)$$

where $A_{v,\text{sat}}$ and $B_{v,\text{sat}}$ are fitting constants that are given in Table II.

Eq. (10)-(11)	α	β_0	β_{exp}
electrons $\langle 100 \rangle$ ($T > 130$ K)	0	2.0	0.10
electrons $\langle 111 \rangle$	0	2.0	0.15
holes $\langle 111 \rangle$	0	0.1	0.06
holes $\langle 111 \rangle$	0	1.5	0.35

Eq. (12)	$A_{v,\text{sat}}$ (cm/s)	$B_{v,\text{sat}}$ (cm/s)
electrons $\langle 100 \rangle$	1.60×10^7	1.03×10^7
electrons $\langle 111 \rangle$	1.17×10^7	6.56×10^6
holes $\langle 100 \rangle$	1.24×10^7	6.48×10^6
holes $\langle 111 \rangle$	9.86×10^6	4.20×10^6

Table II: Constants used for calculating field dependent carrier mobility for electrons and holes in the $\langle 100 \rangle$ and $\langle 111 \rangle$ direction

A comparison of the extended Canali for electrons and holes in the $\langle 100 \rangle$ and $\langle 111 \rangle$ direction for germanium can be seen in Fig. 4. For the electron velocity in the $\langle 100 \rangle$ direction, the inbuilt TCAD mobility degradation model was employed. From the data, it can be seen that the models predict the hole velocity well for both directions in p-type germanium, but there is a significant discrepancy between the data and model in the $\langle 100 \rangle$ for electrons at low temperatures.

When considering the electron mobility within the $\langle 100 \rangle$ direction, it was found that, although the inbuilt models can be adapted to take into account the negative differential mobility, there was a considerable discrepancy at low fields and low temperatures between the model and the data. For the electron velocity in the $\langle 100 \rangle$, the current models fare poorly at lower temperatures and low fields. Looking further into the velocity characteristics, it was found that a better model to describe the velocity characteristics can be made by considering a harmonic average of the extended Canali model and a high field scattering term.

Similarly to the Philips unified mobility model, the new proposed model can be implemented through the harmonic averaging of the extended Canali model and a High-Field scattering factor given by

$$\mu_{\text{HF}}(F) = \frac{A}{F(BF + 2 \times 10^{-7})} \quad (13)$$

where A and B are fitting parameters. A comparison of the new model to experimental data can be seen in Fig. 5. For the fit, it was found that A and B remained temperature independent above 45 K and increased due to the increased negative differential mobility at lower temperatures. The temperature dependence of v_{sat} and β did not follow the original model and were found to be better modelled quadratically as shown in the figure. Using the new model, it can be seen that the temperature dependence of the electron velocity in the $\langle 100 \rangle$ direction of germanium can be recreated from 8 K to room temperature with knowledge of the low field mobility.

V. CONCLUSION

The models presented predict the temperature and doping dependence of the free carrier concentration for both uncompensated and compensated germanium. For the carrier mobility, it has been shown that electron and hole mobility in germanium can be modelled through the adaption of the Philips unified mobility model that is already pre-built into TCAD. The reduction of the carrier mobility at high fields has been modelled based on experimental data considering the transferred electron effect which occurs for electrons in germanium at temperatures below 130 K in the $\langle 100 \rangle$ direction. Using the models presented here and where appropriate the transverse field models presented elsewhere, the conductivity and transfer characteristics of germanium detectors, CMOS and high power devices for emerging room temperature and cryogenic applications can now be predicted and simulated improving optimisation and testing speeds for manufacturers and researchers.

REFERENCES

- [1] Z. Pan, L. An, and C. Wen, "Recent advances in fuel cells based propulsion systems for unmanned aerial vehicles," *Applied Energy*, vol. 240, no. February, pp. 473–485, Apr 2019, doi: [10.1016/j.apenergy.2019.02.079](https://doi.org/10.1016/j.apenergy.2019.02.079).
- [2] E. Solomin, I. Kirpichnikova, R. Amerkhanov, D. Korobotov, M. Lutovats, and A. Martyanov, "Wind-hydrogen standalone uninterrupted power supply plant for all-climate application," *International Journal of Hydrogen Energy*, vol. 44, no. 7, pp. 3433–3449, Feb 2019, doi: [10.1016/j.ijhydene.2018.12.001](https://doi.org/10.1016/j.ijhydene.2018.12.001).
- [3] I. Aschilean, M. Varlam, M. Culcer, M. Iliescu, M. Raceanu, A. Enache, M. Raboaca, G. Rasoi, and C. Filote, "Hybrid Electric Powertrain with Fuel Cells for a Series Vehicle," *Energies*, vol. 11, no. 5, p. 1294, May 2018, doi: [10.3390/en11051294](https://doi.org/10.3390/en11051294).
- [4] J. Qi, X. Yang, X. Li, K. Tian, Z. Mao, S. Yang, and W. Song, "Temperature Dependence of Dynamic Performance Characterization of 1.2-kV SiC Power mosfets Compared With Si IGBTs for Wide Temperature Applications," *IEEE Transactions on Power Electronics*, vol. 34, no. 9, pp. 9105–9117, Sep 2019, doi: [10.1109/TPEL.2018.2884966](https://doi.org/10.1109/TPEL.2018.2884966).
- [5] M. C. Gonzalez, L. W. Kohlman, and A. J. Trunek, "Cryogenic Parametric Characterization of Gallium Nitride Switches," NASA Glenn Research Center, Cleveland, Tech. Rep., Oct 2018.
- [6] M. Jhabvala and S. R. Babu, "Development of Cryogenic Ge JFETs—III," in *Fourth European Workshop on Low Temperature Electronics*, no. June 2000, Noordwijk, 2000, pp. 105–111.
- [7] N. Das, C. Monroy, and M. Jhabvala, "Germanium junction field effect transistor for cryogenic applications," *Solid-State Electronics*, vol. 44, no. 6, pp. 937–940, Jun 2000, doi: [10.1016/S0038-1101\(00\)00013-7](https://doi.org/10.1016/S0038-1101(00)00013-7).
- [8] P. P. Debye and E. M. Conwell, "Electrical Properties of N-Type Germanium," *Physical Review*, vol. 93, no. 4, pp. 693–706, Feb 1954, doi: [10.1103/PhysRev.93.693](https://doi.org/10.1103/PhysRev.93.693).
- [9] H. Fritzsche, "Resistivity and Hall Coefficient of Antimony-Doped Germanium at Low Temperatures," *Journal of Physics and Chemistry of Solids*, vol. 6, no. 1, pp. 69–80, Jul 1958, doi: [10.1016/0022-3697\(58\)90220-8](https://doi.org/10.1016/0022-3697(58)90220-8).
- [10] D. M. Finlayson, V. A. Johnson, and F. M. Shipley, "Interpretation of the Low Temperature Hall Curve of a Degenerate Germanium Sample," *Physical Review*, vol. 87, no. 6, pp. 1141–1142, Sep 1952, doi: [10.1103/PhysRev.87.1141](https://doi.org/10.1103/PhysRev.87.1141).
- [11] H. Fritzsche and M. Cuevas, "Impurity Conduction in Transmutation-Doped p-Type Germanium," *Physical Review*, vol. 119, no. 4, pp. 1238–1245, Aug 1960, doi: [10.1103/PhysRev.119.1238](https://doi.org/10.1103/PhysRev.119.1238).
- [12] C. J. Glassbrenner and G. A. Slack, "Thermal Conductivity of Silicon and Germanium from 3K to the Melting Point," *Physical Review*, no. 4A, pp. A1058–A1069, May, doi: [10.1103/PhysRev.134.A1058](https://doi.org/10.1103/PhysRev.134.A1058).
- [13] S. Ganti, P. J. King, E. Arac, K. Dawson, M. J. Heikkilä, J. H. Quilter, B. Murdoch, P. Cumpson, and A. O'Neill, "Voltage Controlled Hot Carrier Injection Enables Ohmic Contacts Using Au Island Metal Films on Ge," *ACS Applied Materials & Interfaces*, vol. 9, no. 33, pp. 27 357–27 364, Aug 2017, doi: [10.1021/acsami.7b06595](https://doi.org/10.1021/acsami.7b06595).
- [14] H. Liu, G. Han, Y. Xu, Y. Liu, T.-J. K. Liu, and Y. Hao, "High Mobility Ge pMOSFETs with Crystalline ZrO₂ Dielectric," *IEEE Electron Device Letters*, vol. 40, no. 3, pp. 371–374, Mar 2019, doi: [10.1109/LED.2019.2895856](https://doi.org/10.1109/LED.2019.2895856).
- [15] R. Zhang, X. Yu, M. Takenaka, and S. Takagi, "Impact of post-deposition annealing ambient on the mobility of Ge nMOSFETs with 1-nm EOT Al₂O₃/GeO_x/Ge gate-stacks," *IEEE Transactions on Electron Devices*, vol. 63, no. 2, pp. 558–564, Feb 2016, doi: [10.1109/TED.2015.2509961](https://doi.org/10.1109/TED.2015.2509961).
- [16] R. Singh and B. Baliga, "Analysis and optimization of power MOSFETs for cryogenic operation," *Solid-State Electronics*, vol. 36, no. 8, pp. 1203–1211, Aug 1993, doi: [10.1016/0038-1101\(93\)90202-2](https://doi.org/10.1016/0038-1101(93)90202-2).
- [17] D. M. Brown and R. Bray, "Analysis of Lattice and Ionized Impurity Scattering in p-Type Germanium," *Physical Review*, vol. 127, no. 5, pp. 1593–1602, Sep 1962, doi: [10.1103/PhysRev.127.1593](https://doi.org/10.1103/PhysRev.127.1593).
- [18] B.-I. Ho, "Microwave Hall mobilities of holes in germanium," Ph.D. dissertation, Iowa State University, Jan 1966.
- [19] G. L. Pearson and J. Bardeen, "Electrical Properties of Pure Silicon and Silicon Alloys Containing Boron and Phosphorus," *Physical Review*, vol. 75, no. 5, pp. 865–883, Mar 1949, doi: [10.1103/PhysRev.75.865](https://doi.org/10.1103/PhysRev.75.865).
- [20] S. Kagamihara, H. Matsuura, T. Hatakeyama, T. Watanabe, M. Kushibe, T. Shinohe, and K. Arai, "Parameters required to simulate electric characteristics of SiC devices for n-type 4H-SiC," *Journal of Applied Physics*, vol. 96, no. 10, pp. 5601–5606, Nov 2004, doi: [10.1063/1.1798399](https://doi.org/10.1063/1.1798399).
- [21] J. De Boer and W. Van Geel, "Rotgrenze des inneren photoeffektes und ablösungsarbeit bei halbleitern," *Physica*, vol. 2, no. 1-12, pp. 286–298, Jan 1935, doi: [10.1016/S0031-8914\(35\)90091-X](https://doi.org/10.1016/S0031-8914(35)90091-X).
- [22] C. Jacoboni, F. Nava, C. Canali, and G. Ottaviani, "Electron drift velocity and diffusivity in germanium," *Physical Review B*, vol. 24, no. 2, pp. 1014–1026, Jul 1981, doi: [10.1103/PhysRevB.24.1014](https://doi.org/10.1103/PhysRevB.24.1014).
- [23] E. J. Ryder, "Mobility of Holes and Electrons in High Electric Fields," *Physical Review*, vol. 90, no. 5, pp. 766–769, Jun 1953, doi: [10.1103/PhysRev.90.766](https://doi.org/10.1103/PhysRev.90.766).
- [24] G. Ottaviani, C. Canali, F. Nava, and J. W. Mayer, "Hole drift velocity in high-purity Ge between 8 and 220 K," *Journal of Applied Physics*, vol. 44, no. 6, pp. 2917–2918, Jun 1973, doi: [10.1063/1.1662678](https://doi.org/10.1063/1.1662678).
- [25] L. Reggiani, C. Canali, F. Nava, and G. Ottaviani, "Hole drift velocity in germanium," *Physical Review B*, vol. 16, no. 6, pp. 2781–2791, Sep 1977, doi: [10.1103/PhysRevB.16.2781](https://doi.org/10.1103/PhysRevB.16.2781).
- [26] D. Klaassen, "A unified mobility model for device simulation—I. Model equations and concentration dependence," *Solid-State Electronics*, vol. 35, no. 7, pp. 953–959, Jul 1992, doi: [10.1016/0038-1101\(92\)90325-7](https://doi.org/10.1016/0038-1101(92)90325-7).
- [27] E. Fistul, VI and Iglitsyn, MI and Omelyanovskii, "Mobility of electrons in germanium strongly doped with arsenic," *Soviet Physics-Solid State*, vol. 4, no. 4, pp. 784–785, 1962.
- [28] L. Golikova, OA and Moizhes, B Ya and Stilbans, "Hole mobility of germanium as a function of concentration and temperature," *Soviet Physics-Solid State*, vol. 3, no. 10, pp. 2259–2265, 1962.
- [29] M. B. Prince, "Drift mobilities in semiconductors. i. germanium," *Phys. Rev.*, vol. 92, pp. 681–687, Nov 1953, doi: [10.1103/PhysRev.92.681](https://doi.org/10.1103/PhysRev.92.681).
- [30] E. G. S. Paige, "The Drift Mobility of Electrons and Holes in Germanium at Low Temperatures," *Journal of Physics and Chemistry of Solids*, vol. 16, pp. 207–219, Nov 1960, doi: [10.1016/0022-3697\(60\)90151-7](https://doi.org/10.1016/0022-3697(60)90151-7).
- [31] C. Canali, G. Majni, R. Minder, and G. Ottaviani, "Electron and hole drift velocity measurements in silicon and their empirical relation to electric field and temperature," *IEEE Transactions on Electron Devices*, vol. 22, no. 11, pp. 1045–1047, Nov 1975, doi: [10.1109/T-ED.1975.18267](https://doi.org/10.1109/T-ED.1975.18267).